Spin-dynamics simulations of the triangular antiferromagnetic *XY* model

Kwangsik Nho and D. P. Landau

Center for Simulational Physics, University of Georgia, Athens, Georgia 30602

(Received 10 May 2002; published 4 November 2002)

Using Monte Carlo and spin-dynamics methods, we have investigated the dynamic behavior of the classical, antiferromagnetic *XY* model on a triangular lattice with linear sizes $L \leq 300$. The temporal evolutions of spin configurations were obtained by solving numerically the coupled equations of motion for each spin using fourth-order Suzuki-Trotter decompositions of exponential operators. From space- and time-displaced spin-spin correlation functions and their space-time Fourier transforms we obtained the dynamic structure factor $S(\mathbf{q}, w)$ for momentum $\mathbf{q}$ and frequency ω. Below T_{KT} (Kosterlitz-Thouless transition), both the in-plane (S^{xx}) and out-of-plane (S^{zz}) components of $S(\mathbf{q}, \omega)$ exhibit very strong and sharp spin-wave peaks. Well above T_{KT}, S^{xx} and S^{zz} apparently display a central peak, and spin-wave signatures are still seen in S^{zz}. In addition, we also observed an almost dispersionless domain-wall peak at high ω below T_c (Ising transition), where long-range order appears in the staggered chirality. Above T_c, the domain-wall peak disappears for all q. The line shape of these peaks is captured reasonably well by a Lorentzian form. Using a dynamic finite-size scaling theory, we determined the dynamic critical exponent $z = 1.002(3)$. We found that our results demonstrate the consistency of the dynamic finite-size scaling theory for the characteristic frequency ω_m and the dynamic structure factor $S(\mathbf{q}, \omega)$ itself.

I. INTRODUCTION

The study of the dynamic properties of classical spin systems has been extensively carried out using both theoretical and simulational approaches. In their work on the theory of dynamic critical phenomena,[1] Hohenberg and Halperin proposed a number of different dynamic universality classes based upon the conservation laws. The dynamic critical behavior is describable in terms of a dynamic critical exponent *z*, which gives rise to different dynamic universality classes: *z* depends on the conservation laws, lattice dimension, and the static critical exponents. Now spin-dynamics simulations have become a mature method for probing the time-dependent behavior of magnetic systems (see Ref. 2 for a recent review). This approach has resulted in high-quality dynamic critical exponent estimates for numerous models. In a recent high-resolution spin-dynamics study,[3] Tsai *et al.* made direct, quantitative comparison of both the dispersion curve and the line shapes obtained from their simulation data with recent experimental results for $RbMnF_3$ using the Heisenberg antiferromagnet model and a newly developed approach of higher-order decomposition time integration methods[4] and obtained a good agreement.

In this paper we consider the classical two-dimensional (2D) antiferromagnetic *XY* model on a triangular lattice (TAFXY). This frustrated 2D spin system has received much attention during the last decade.[5–11] The TAFXY model displays rich low-temperature phase structures and critical phenomena because frustration introduces additional discrete symmetries resulting from the chiral degrees of freedom. The ground states of this model are composed of three interpenetrating sublattices with lattice vectors of length $\sqrt{3}$. Spins on each sublattice are ferromagnetically ordered and spins on different sublattices are oriented $\pm 2\pi/3$ with respect to each other. The TAFXY has a continuous U(1) symmetry associated with global spin rotations and a discrete Z_2 symmetry because of the double degeneracy of the ground-state chirality configurations. This model has two order parameters: the staggered in-plane magnetization and the staggered chirality. There have been ongoing controversies concerning phase transitions and the nature of the phase transitions. Some[5,6] suggested that the system undergoes a single phase transition, generally yielding a non-Ising critical exponent; however, others[7–11] supported a double-phase-transition scenario with a Kosterlitz-Thouless- (KT-) like transition followed by a second-order chirality-lattice melting transition at a slightly higher temperature. In addition to spin waves and vortices, which are fundamental excitations in the ferromagnetic or antiferromagnetic *XY* model on a bipartite lattice, the triangular antiferromagnetic *XY* model has other excitations associated with domain-wall formation between two different ground states in view of the chirality configuration of ground states.[8]

A good experimental realization of the frustrated antiferromagnetic *XY* model on a stacked triangular lattice is ABX_3-type halides (like $CsNiCl_3$, $CsMnBr_3$, and $CsCuCl_3$).[12,13] The magnetic B^{2+} ions form a triangular antiferromagnet within the *ab* planes and a ferromagnetic coupling along the *c* direction produces three-dimensional order.

While the static critical behavior of the TAFXY model has been the subject of much interest during the last decade, a theoretical study of the dynamic critical behavior has not been carried out for the TAFXY model.

In the present work, we have studied the dynamic behavior of the TAFXY model using Monte Carlo and spin-dynamic (MC-SD) methods. Although in the usual planar *XY* model each spin has two components, here we use the three-component *XY* model in order to study the real dynamics. These two models belong to the same static universality class,[14,15] but the planar *XY* model will not have true dynamical behavior.[1]

The estimates for T_{KT} and T_c used here are taken from a

recent high-precision MC study where the critical temperature T_c associated with the chirality phase transition and the KT transition temperature T_{KT} associated with unbinding of vortex pairs have been determined as $T_c = 0.412(5)J/k_B$ and $T_{KT} = 0.403(1)J/k_B$.[10]

II. MODEL AND SIMULATION METHOD

We will first briefly describe the model and the numerical method used here and show how the dynamic structure factor is computed. The classical antiferromagnetic *XY* model is described by the following form:

$$H = J \sum_{\langle ij \rangle} (S_i^x S_j^x + S_i^y S_j^y), \qquad (1)$$

where the summation is over all nearest neighbors, $\mathbf{S}_i = (S_i^x, S_i^y, S_i^z)$ is a three-dimensional classical spin of unit length at site i, and J is the positive (antiferromagnetic) coupling constant between nearest-neighbor pairs of spins. We consider triangular lattices of size $L \times L$ along the primitive vector directions $(\hat{e}_x, \frac{1}{2}\hat{e}_x + (\sqrt{3}/2)\hat{e}_y)$, containing $N = L^2$ sites and $2N$ elementary triangles. In our calculations, periodic boundary conditions are applied along the primitive vector directions.

We use a hybrid Monte Carlo procedure which consists of a combination of the Metropolis update[16] and the overrelaxation algorithm[17] (see also Ref. 18). One hybrid Monte Carlo step consists of two Metropolis and eight overrelaxation updates.[19,20] Using this hybrid algorithm, we generated approximately 700–8500 equilibrium configurations at a given temperature. Typically 1000 hybrid Monte Carlo steps were used to generate each equilibrium configuration, which is then evolved using the equations of motion given by

$$\frac{d}{dt}\mathbf{S}_i = \frac{\partial H}{\partial \mathbf{S}_i} \times \mathbf{S}_i. \qquad (2)$$

Starting from a particular initial spin configuration, we performed numerical integration of these equations of motion using a recently developed fourth-order Suzuki-Trotter decomposition method,[4] and the integration is carried out to a maximum time t_{max}, typically of the order of $t_{max}J = 680$ and $t_{cutoff}J = 600$, with a time step of $\delta t = 0.2J^{-1}$. We compute the thermal average of a time-dependent observable by averaging over all the values of the observable obtained by evolving all independent initial equilibrium configurations.

The dynamic structure factor $S^{kk}(\mathbf{q}, \omega)$ is the space-time Fourier transform of the position- and time-displaced spin-spin correlation function. It is defined for momentum transfer $\mathbf{q}$ and frequency transfer ω as follows:[19]

$$S^{kk}(\mathbf{q}, \omega) = \sum_{\mathbf{r}, \mathbf{r}'} e^{i\mathbf{q} \cdot (\mathbf{r} - \mathbf{r}')} \int_{-\infty}^{+\infty} e^{i\omega t} C^{kk}(\mathbf{r} - \mathbf{r}', t) \frac{dt}{2\pi}, \qquad (3)$$

where $k = x$, y, or z is the spin component and the space-displaced, time-displaced spin-spin correlation function is given by

$$C^{kk}(\mathbf{r} - \mathbf{r}', t - t') = \langle S_{\mathbf{r}}^k(t) S_{\mathbf{r}'}^k(t') \rangle - \langle S_{\mathbf{r}}^k(t) \rangle \langle S_{\mathbf{r}'}^k(t') \rangle. \qquad (4)$$

The dynamic critical exponent z can be determined by using the dynamic finite-size scaling theory developed by Chen and Landau[19] for deterministic systems:

$$\frac{\omega S_L^{kk}(\mathbf{q}, \omega)}{\chi_L^{kk}(\mathbf{q})} = G^{kk}(\omega L^z, qL), \qquad (5)$$

where we do not introduce a frequency resolution function in order to smoothen the effects of the finite length of time integration because of very long integration times used in our spin dynamics. $\chi_L^{kk}(\mathbf{q})$ is the total integrated intensity given by

$$\chi_L^{kk}(\mathbf{q}) = \int_{-\infty}^{\infty} S_L^{kk}(\mathbf{q}, \omega) d\omega. \qquad (6)$$

The characteristic frequency $\omega_m^{kk}(qL)$ is a median frequency determined by the constraint

$$\frac{1}{2} \chi_L^{kk}(\mathbf{q}) = \int_{-\omega_m^{kk}}^{\omega_m^{kk}} S_L^{kk}(\mathbf{q}, \omega) d\omega. \qquad (7)$$

In the dynamic scaling theory, the finite-size scaling expression for the median frequency ω_m^{kk} is given by

$$\omega_m^{kk} = L^{-z} \Omega(qL). \qquad (8)$$

Using Eq. (8), we estimate the dynamic critical exponent z from the slope of a graph of $\log(\omega_m^{kk})$ versus $\log(L)$ at fixed value of qL, and we test the dynamic finite-size scaling theory using Eq. (5).

III. RESULTS AND DISCUSSION

We first compare the behavior of the dynamic structure factor $S^{kk}(q, \omega)$ at several different temperatures, where k refers to the x (in-plane) or z (out-of-plane) component and we were limited to the [11] reciprocal lattice direction, i.e., $\mathbf{q} = (q, q)$, with q determined by the periodic boundary conditions

$$q = \frac{4\pi}{L} n_q, \quad n_q = 1, 2, \ldots, \frac{L}{3}. \qquad (9)$$

Figure 1 shows the temperature dependence of the dynamic structure factor $S^{kk}(q, \omega)$ for a lattice size of $L = 240$ and a particular momentum $q = 2\pi/15$. For $T \lesssim T_{KT}$ our results for the dynamic structure factor S^{xx} show a very strong spin-wave and a central peak which are visible as pronounced peaks at the spin-wave frequency $\omega(q)$ and at $\omega = 0$, respectively. S^{zz} has structures with less intensity than S^{xx} [note the change in scale between Figs. 1(a) and 1(b)]. There is a sharp spin-wave peak and no central peaks are visible in S^{zz}. The positions of the spin-wave peaks are the same for S^{xx} and S^{zz}, and as the temperature increases, the spin-wave peak broadens, its position moves towards lower ω, and its amplitude decreases. Above T_{KT}, S^{xx} and S^{zz}
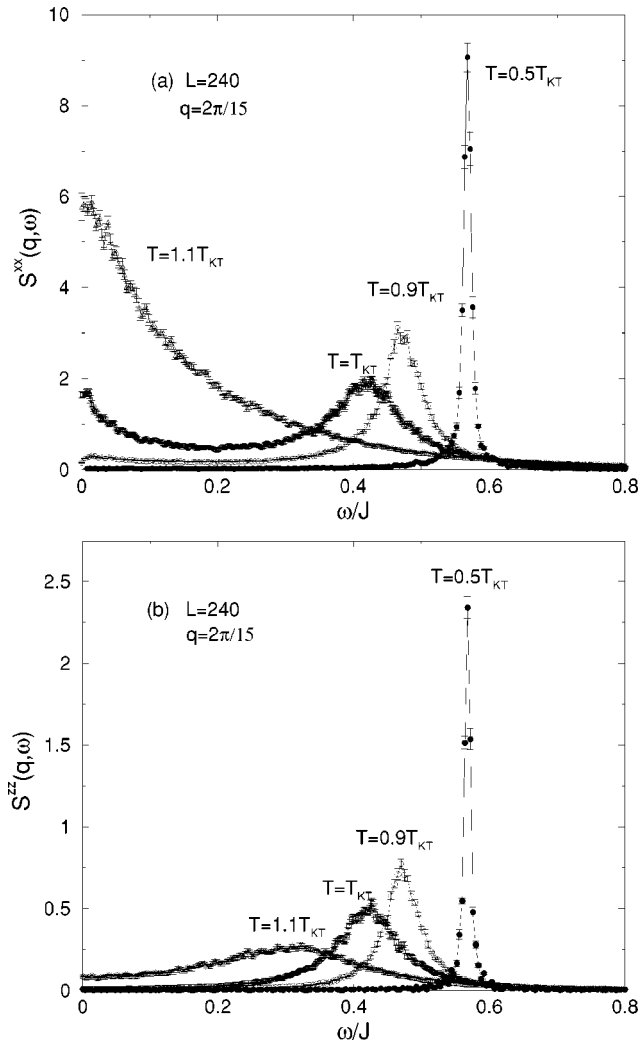
FIG. 1. Temperature dependence of the dynamic structure factor $S^{kk}(q,\omega)$. $L=240$ and $q=2\pi/15$ in the [11] direction in all cases: (a) in-plane component and (b) out-of-plane component.

apparently display a central peak, but spin-wave signatures are still visible in S^{zz}. The same qualitative behavior was observed in spin-dynamics simulations of the 2D classical XY model on a square lattice.[14]

As has been pointed out by Lee $et\ al.$,[8] in addition to spin waves, there is another type of elementary excitation associated with domain-wall formation between regions with opposite staggered chirality. In order to observe the dynamic effects of the destruction of chirality order, we investigate the temperature dependence of the dynamic structure factor S^{xx} at high frequencies. We illustrate this in Fig. 2. The intensity of the domain-wall peak is 10^{-2} of that of the spin-wave peak at small q [note the change in scale between Figs. 1(a) and 2]. The relative intensity decreases at large q. For clarity, a frequency resolution function with $\delta\omega=1.2\pi/t_{cutoff}$ is used to smooth the oscillations due to the finite t_{max}. Below T_c, where long-range order appears in the staggered chirality, we observe an almost dispersionless domain-wall peak at high ω typical of an Ising model. As the temperature approaches the chirality transition T_c from below, the domain-wall peak broadens and its relative intensity de-
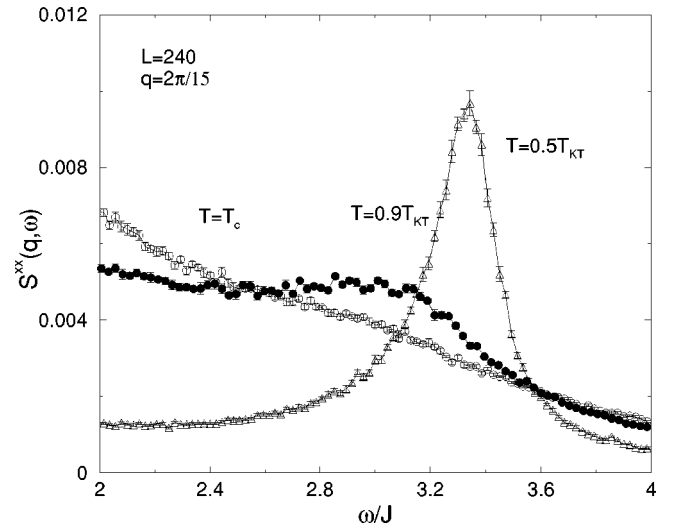

FIG. 2. Temperature dependence of the dynamic structure factor $S^{xx}(q,\omega)$ at high frequencies. $L=240$ and $q=2\pi/15$ in the [11] direction in all cases. For clarity, a frequency resolution function is used to smoothen the oscillations due to the finite t_{max}. We can see a domain-wall peak for $T<T_c$. The peak broadens as the temperature increases. However, the domain-wall peak disappears at $T \geqslant T_c$.

creases. The domain-wall peak disappears for all q above T_c. This result indicates the presence of an Ising-like phase transition connected with the loss of chirality order. Figure 3 shows $S^{xx}(q,\omega)$ for three different system sizes with the same value of $q=2\pi/15$ at high ω in order to see the finite-size effects of the domain-wall peak. The intensity of the domain-wall peak does not depend on lattice size, the data essentially collapse onto a single curve, and finite-size effects are not visible, whereas the intensity of the spin-wave peak depends strongly on lattice size.
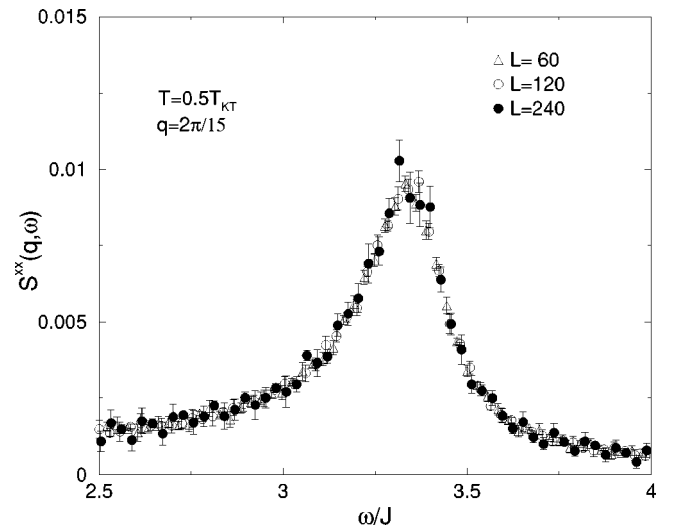

FIG. 3. Lattice size dependence of dynamic structure factor $S^{xx}(q,\omega)$ around the domain-wall peak position at fixed momentum $q=2\pi/15$ in the [11] direction at $T=0.5T_{KT}$. The intensity of the domain-wall peak does not depend on lattice size and the data essentially collapse onto a single curve.
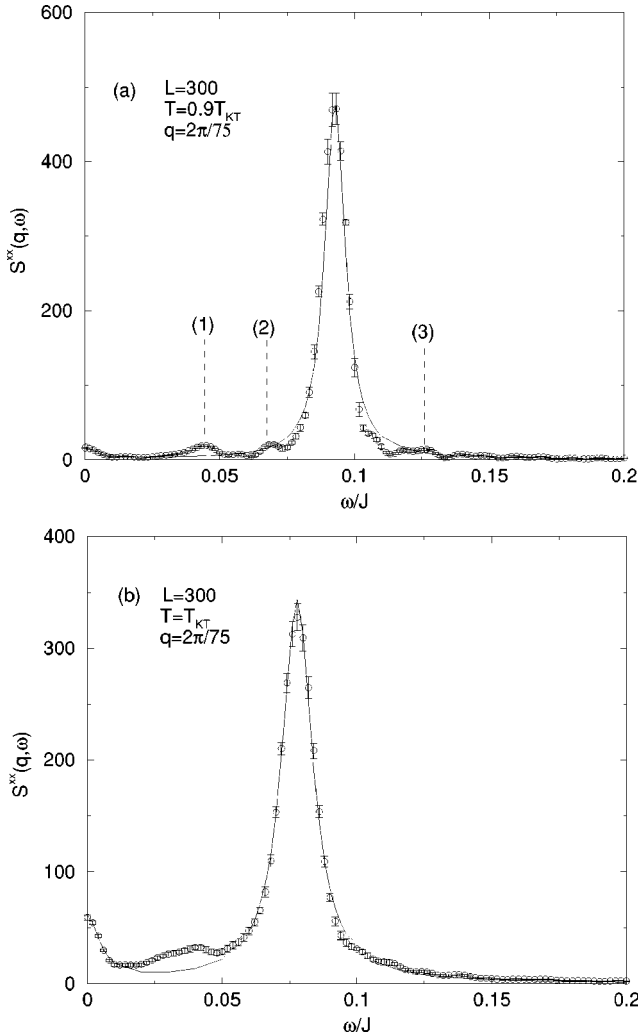
FIG. 4. In-plane component S^{xx} of the dynamic structure factor for $L=300$. (a) $T=0.9T_{KT}$ and (b) $T=T_{KT}$ at $q=2\pi/75$ in the [11] direction in all cases. The symbols represent simulation data and the solid line is a fit with the multiple Lorentzian function given in Eq. (10).

The in-plane dynamic structure factor $S^{xx}(\mathbf{q},\omega)$ for the 2D *XY* model below the topological transition temperature T_{KT} was analyzed by Villain,[21] Moussa and Villain,[22] and Nelson and Fisher.[23] They found that $S^{xx}(\mathbf{q},\omega)$ has spin-wave peaks diverging at the spin-wave frequency $\omega_p(\mathbf{q})$. Menezes *et al.*[24] calculated $S(\mathbf{q},\omega)$ and found a diverging spin-wave peak similar to that of Nelson and Fisher and a logarithmically diverging central peak. However Evertz and Landau[14] found that their MC-SD data for the shape of $S(\mathbf{q},\omega)$ are not well described around the spin-wave peak by the above theoretical predictions.

Mertens *et al.*[25,26] calculated $S(\mathbf{q},\omega)$ above T_{KT} and found a Lorentzian central peak for S^{xx} and a Gaussian central peak for S^{zz}. Very recently, Wysin *et al.*[27] calculated $S(\mathbf{q},\omega)$ and found nondivergent spin-wave peaks and weak peaks on both sides of the spin-wave peaks. Below T_{KT}, these theoretical approaches motivated us to fit the line shape of the dynamic structure factor S^{xx} to a Lorentzian form. We found that the line shape of S^{xx} is reasonably well captured
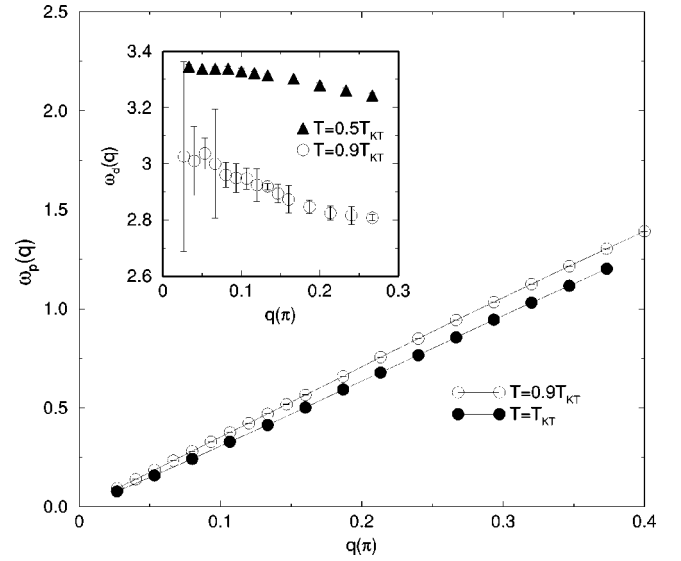

FIG. 5. Dispersion relation $\omega_p(q)$ of the spin-wave peak in $S^{xx}(q,\omega)$ for the [11] direction as a function of momentum. The inset shows the dispersion relation $\omega_d(q)$ of the domain-wall peak.

by a multiple Lorentzian form

$$S^{xx}(q,\omega) = \frac{A\Gamma_1^2}{\Gamma_1^2+\omega^2} + \frac{B\Gamma_2^2}{\Gamma_2^2+(\omega-\omega_p^2)} + \frac{B\Gamma_2^2}{\Gamma_2^2+(\omega+\omega_p^2)}$$
$$+ \frac{C\Gamma_3^2}{\Gamma_3^2+(\omega-\omega_d^2)} + \frac{C\Gamma_3^2}{\Gamma_3^2+(\omega+\omega_d^2)}, \quad (10)$$

where the first term corresponds to the central peak, the next two terms are from the spin-wave creation and annihilation peaks at $\omega=\pm\omega_p$, and the last two terms are contributions from the domain-wall peaks at $\omega=\pm\omega_d$. In order to fit the simulated line shapes to the Lorentzian form, Eq. (10), we used a frequency range $0\leqslant\omega\leqslant5$. We find that the Lorentzian line shapes fit our simulation data reasonably well. Illustrations of the fits using Eq. (10) to the simulated line shapes at $T=0.9T_{KT}$ and at T_{KT} are shown in Fig. 4. In the figure the symbols represent our simulation data and the solid line is a fit with the Lorentzian function given in Eq. (10). In Figs. 4(a) and 4(b), we find additional small peaks on both sides of the spin-wave peak. One simple explanation which is consistent with the data is the presence of two-spin-wave peaks. We could see that the position of these extra peaks corresponded to frequencies of two-spin-wave addition and difference peaks [marked as (1), (2), and (3) in Fig. 4(a)]. These dynamical features have been noticed in earlier MC-SD simulations[3,14,28] and a theoretical approach.[27] As we did not generalize Eq. (10) to include the extra peaks, this extra structure causes the line shape to depart from a Lorentzian form.

The dispersion relations $\omega_p(q)$ of the spin-wave peak and $\omega_d(q)$ of the domain-wall peak can be obtained from the above Lorentzian fit. Figure 5 shows the dispersion curves as a function of momentum. The inset shows the dispersion relation $\omega_d(q)$ at $T=0.5T_{KT}$ and $T=0.9T_{KT}$, where obtaining a good $\omega_d(q)$ is difficult because of the small peak
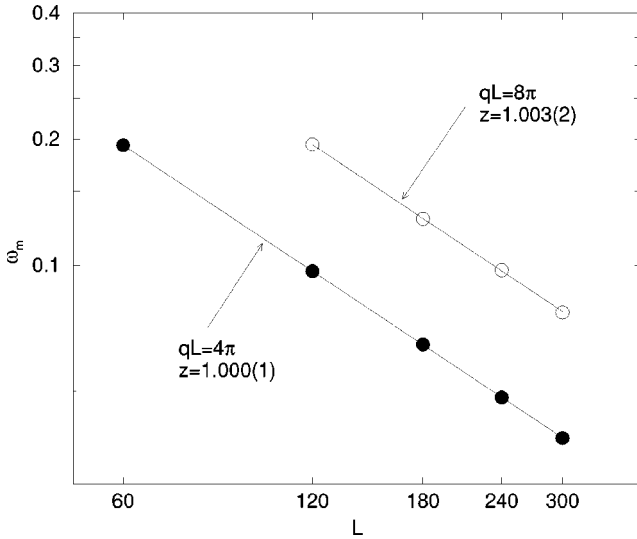
FIG. 6. Finite-size scaling plot for the median frequency ω_m^{xx} at $T=T_{KT}$. The dynamic critical exponent value obtained from the slope of the log-log plot is $z=1.000(1)$ for $n=1$ using all lattice sizes and $z=1.003(2)$ for $n=2$ using the largest four lattice sizes. The solid lines display a fit to a straight line. Statistical errors of the data are smaller than the symbol sizes.

height and the broadening of the domain-wall peak (see Fig. 2). As expected, $\omega_p(q)$ is linear for small q and $\omega_d(q)$ is approximately constant.

The dynamic critical exponent z can be extracted from the finite-size scaling of the characteristic frequency ω_m, as described in a previous section. We calculated $\omega_m^{xx}(qL)$ using S^{xx} with $qL=4\pi(n=1)$ and $qL=8\pi(n=2)$ for several lattice sizes at T_{KT}. The log-log plot of the characteristic frequency ω_m^{xx} as a function of the lattice size L is shown in Fig. 6 where the estimated error bars for individual points are smaller than the symbol sizes. The solid lines display a fit to linear behaviors. From the slope of a $\log(\omega_m^{xx})$ vs $\log(L)$ graph, we obtained the dynamic critical exponent $z=1.000$ ± 0.001 for $n=1$ using all lattice sizes and $z=1.003$ ± 0.002 for $n=2$ using only the largest four lattice sizes. Within their respective error bars, the two estimates for z agree. Our final estimate for the dynamic critical exponent is $z=1.002(3)$, where the error bar reflects the fluctuations in the different estimates of z. Our determined value for z is in excellent agreement with theoretical prediction[1] and with that of the 2D *XY* model on a square lattice, $z=1.00$ ± 0.04.[14] For comparison, we proceeded to estimate the dynamic critical exponent z at T_c. We obtained the dynamic critical exponent $z=1.051\pm0.005$ for $n=1$ (not shown). However, this does not mean that it should be $z=1$ at $T=T_c$. There is no theoretical argument why z should also equal 1 at this transition. We then calculated $\omega_m^{kk}(qL)$ using S^{kk} for all q in the [11] direction and all lattice sizes L and we graphed $\omega_m^{kk}L^z$ as a function of qL^z for $T\le T_{KT}$ using $z=1.0$. This graph is shown in Fig. 7. In the figure, statistical errors of the data are smaller than the symbol sizes. As we know, the dispersion curve flattens for each finite lattice size when q becomes large; therefore, the data start to move away from the asymptotic behavior at progressively larger values
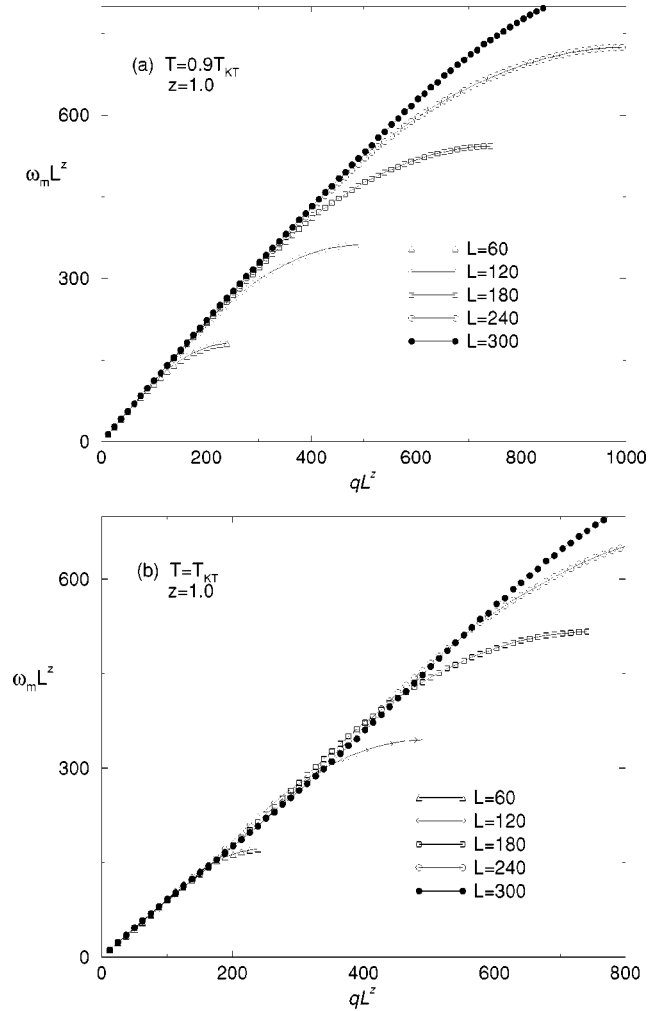

FIG. 7. Finite-size scaling of the median frequency ($\omega_m^{xx}L^z$ as a function of qL^z) at (a) $T=0.9T_{KT}$ and (b) T_{KT} using $z=1.0$. The data for ω_m^{xx} show good scaling behavior for $T\le T_{KT}$. Statistical errors of the data are smaller than the symbol sizes.

of qL. The data for ω_m^{xx} show good scaling behavior for $T \le T_{KT}$. The out-of-plane characteristic frequency ω_m^{zz} has the same scaling behavior as the in-plane component at temperatures $T\le T_{KT}$. Interestingly, at $T=T_c$, ω_m^{zz} also shows the same good scaling behavior with $z=1.0$; however, we do not observe similar scaling behavior in ω_m^{xx} at $T=T_c$. The same behavior was observed by spin-dynamics simulation of the 2D *XY* model on a square lattice in a qualitative sense.[14]

We had also attempted to estimate the q dependence of the half-width $\Gamma^{kk}(q)$ of the spin-wave peak in the critical region. Here we expect the simple form $\Gamma^{kk}(q)\sim q^z$. The log-log plot of the half-width $\Gamma^{kk}(q)$ from our simulations is shown in Fig. 8. For $\Gamma^{zz}(q)$, we estimated the error in the fitted parameters by fitting the line shapes using three different ranges of frequency around the spin-wave peak. The fitted parameters varied when different frequency ranges were used in the fit. For $\Gamma^{xx}(q)$, however, as there are three peaks (central, spin-wave, and domain-wall) in $S^{xx}(q,\omega)$ below T_c, obtaining a good fitted parameter was more difficult than $\Gamma^{zz}(q)$. First, the line shape parameters are obtained from
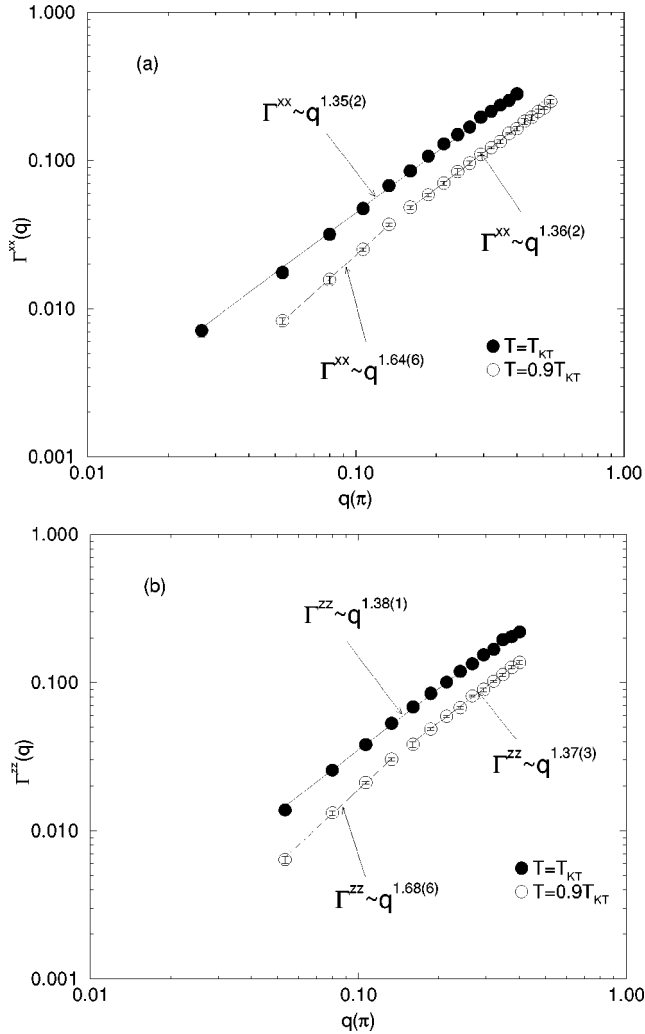
FIG. 8. Linewidths (a) $\Gamma^{xx}(q)$ and (b) $\Gamma^{zz}(q)$ of the spin-wave peak in $S^{kk}(q,\omega)$ for the [11] direction and $L=300$. The solid lines are linear fits to the data points.

FIG. 9. Finite-size scaling of the dynamic structure factor S^{xx} for $z=1.0$, $qL=4\pi$ in the [11] direction, and $T=T_{KT}$. Data points collapse onto the same curve for sufficiently large L. Only the data from small lattices deviate systematically.

cally. Scaling works quite well for all frequencies for lattice sizes $L=240$ and 300. The corresponding plot for $S^{xx}(q,\omega)$ and $qL=4\pi$ at $T=T_c$ is displayed in Fig. 10. The dynamic structure factors for the largest three lattice sizes fall onto a single curve within the bounds of their error bars. Our MC-SD data clearly show that even above T_{KT} the dynamic structure factor scales quite well, consistent with the results of the 2D *XY* model on a square lattice by Evertz and Landau.[14] For the out-of-plane component S^{zz}, we do observe scaling (not shown). Thus we can validate the dynamic finite-size scaling theory.

IV. SUMMARY AND CONCLUSION

We have studied the dynamic critical behavior of the classical 2D antiferromagnetic planar (*XY*) model on a triangu-

the fit to only one frequency range. Using these parameters, the central peak and the domain-wall peak are subtracted. The error is estimated by varying the size of the frequency window around the spin-wave peak. In contrast to our expectation, we observed two different dynamic exponents for two different regions of q in $\Gamma^{kk}(q)$ at $T=0.9T_{KT}$. To check the finite-size effects for the half-width $\Gamma^{kk}(q)$, we have calculated the $\Gamma^{zz}(q)$ at two different lattice sizes $L=240$ and $L=300$. However, we could not see any finite-size effects for the range of the wave vectors that are shown in the figure. In order to check our result, we calculated $\Gamma^{zz}(q)$ for the two-dimensional *XY* model on a square lattice and obtained two different exponents as well (not shown).

In order to test the dynamic finite-size scaling theory of the dynamic structure factor S^{kk} itself through the use of Eq. (5), we plotted $S_L^{kk}(q,\omega)/L^z\chi_L^{kk}(q)$ vs ωL^z for four lattice sizes with the dynamic critical exponent set to $z=1.0$. For $qL=4\pi$ ($n=1$) and $T=T_{KT}$, the resulting scaling plot for $S^{xx}(q,\omega)$ is shown in Fig. 9. Data points collapse onto the same curve for sufficiently large L—namely, lattice sizes $L \geq 240$. Only the data from small lattices deviate systemati-
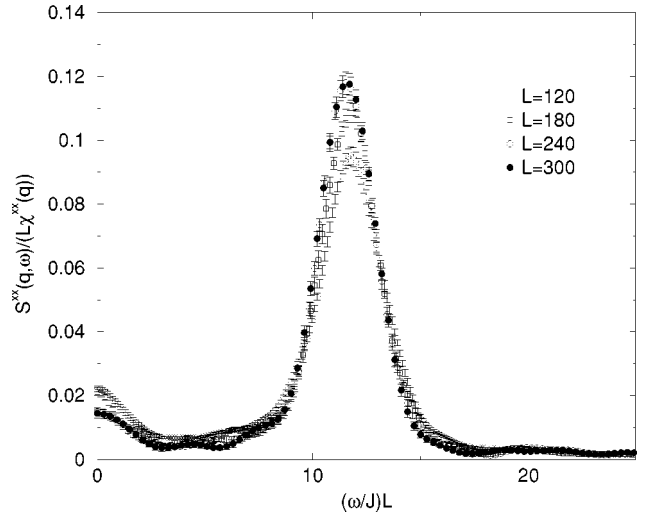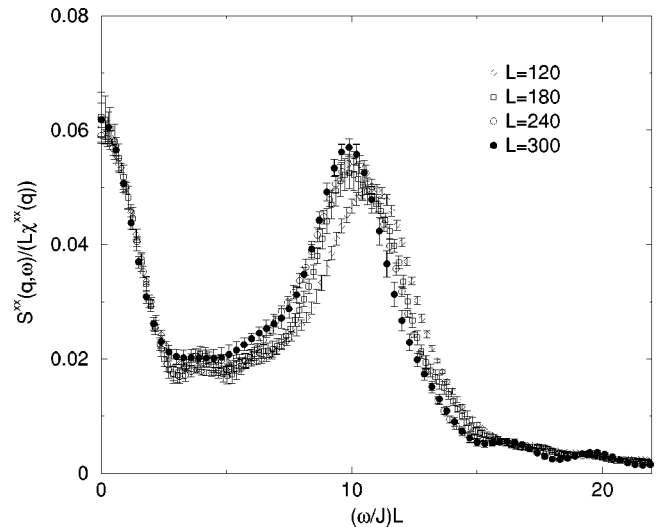

FIG. 10. Finite-size scaling of the dynamic structure factor S^{xx} for $z=1.0$, $qL=4\pi$ in the [11] direction, and $T=T_c$. Data points collapse onto the same curve for sufficiently large L. Only the data from small lattices deviate systematically.

lar lattice using a combination of Monte Carlo methods and spin-dynamics techniques which use recently developed decomposition methods in order to increase the efficiency of the simulations. We have calculated the dynamic structure factor $S^{kk}(q,\omega)$ at temperatures below, at, and above T_c with lattice sizes $L \leq 300$.

At $T \leq T_{KT}$, very strong, sharp spin-wave peaks occur in both the in-plane and out-of-plane components of the dynamic structure factor $S(q,\omega)$. As T increases, the spin-wave peak widens and its position moves towards lower ω. In addition to the spin-wave peak, $S^{xx}(q,\omega)$ displays a central peak and additional two-spin-wave peaks. No central peaks are visible in $S^{zz}(q,\omega)$. Above T_{KT}, $S^{xx}(q,\omega)$ and $S^{zz}(q,\omega)$ apparently display a central peak and spin-wave signatures are still in S^{zz}. In a qualitative sense, the same behavior was observed in spin-dynamics simulations of the 2D XY model on a square lattice.[14]

Below T_c, where long-range order appears in the staggered chirality, we observed an almost dispersionless domain-wall peak at high ω. The domain-wall peak broadens and its intensity decreases as the temperature increases. However, the intensity of the domain-wall peak does not depend on lattice size. The domain-wall peak disappears for all q above T_c.

The line shape of the central, spin-wave, and domain-wall peaks is captured reasonably well by a Lorentzian form. We estimated the dynamic critical exponent z from the finite-size scaling of the characteristic frequency ω_m. Our determined value is $z=1.002(3)$, which is in agreement with that of the 2D XY model on a square lattice $z=1.00(4)$.[14]

Finally, we have examined the dynamic finite-size scaling theory and we found that the characteristic frequency $\omega_m^{kk}(qL)$ and the dynamic structure factor $S^{kk}(q,\omega)$ itself scale very well.

ACKNOWLEDGMENTS

[1] P.C. Hohenberg and B.I. Halperin, Rev. Mod. Phys. **49**, 435 (1977).

[2] D.P. Landau and M. Krech, J. Phys.: Condens. Matter **11**, R179 (1999).

[3] S.H. Tsai, A. Bunker, and D.P. Landau, Phys. Rev. B **61**, 333 (2000).

[4] M. Krech, A. Bunker, and D.P. Landau, Comput. Phys. Commun. **111**, 1 (1998); J. Frank, W. Huang, and B. Leimkuhler, J. Comput. Phys. **133**, 160 (1997).

[5] J. Lee, J.M. Kosterlitz, and E. Granato, Phys. Rev. B **43**, 11 531 (1991).

[6] M. Benakli, H. Zheng, and M. Gabay, Phys. Rev. B **55**, 278 (1997).

[7] S. Miyashita and H. Shiba, J. Phys. Soc. Jpn. **53**, 1145 (1984).

[8] D.H. Lee, J.D. Joannopoulos, J.W. Negele, and D.P. Landau, Phys. Rev. Lett. **52**, 433 (1984); Phys. Rev. B **33**, 450 (1986).

[9] S. Lee and K.C. Lee, Phys. Rev. B **57**, 8472 (1998).

[10] L. Capriotti, R. Vaia, A. Cuccoli, and V. Tognetti, Phys. Rev. B **58**, 273 (1998).

[11] W. Stephan and B.W. Southern, Phys. Rev. B **61**, 11 514 (2000).

[12] H. Serrano-Gonzalez, S.T. Bramwell, K.D.M. Harris, B.M. Kariuki, L. Nixon, I.P. Parkin, and C. Ritter, Phys. Rev. B **59**, 14 451 (1999).

[13] V.P. Plakhty, S.V. Maleyev, J. Kulda, J. Wosnitza, D. Visser, and E. Moskvin, Europhys. Lett. **48**, 215 (1999).

[14] H.G. Evertz and D.P. Landau, Phys. Rev. B **54**, 12302 (1996).

[15] K. Nho and E. Manousakis, Phys. Rev. B **59**, 11 575 (1999).

[16] N. Metropolis, A.W. Rosenbluth, M.N. Rosenbluth, A.M. Teller, and E. Teller, J. Chem. Phys. **21**, 1087 (1953).

[17] F.R. Brown and T.J. Woch, Phys. Rev. Lett. **58**, 2394 (1987); M. Creutz, Phys. Rev. D **36**, 515 (1987).

[18] D. P. Landau and K. Binder, *Monte Carlo Simulations in Statistical Physics* (Cambridge University Press, Cambridge, England, 2000).

[19] K. Chen and D.P. Landau, Phys. Rev. B **49**, 3266 (1994).

[20] A. Bunker, K. Chen, and D.P. Landau, Phys. Rev. B **54**, 9259 (1996).

[21] J. Villain, J. Phys. (Paris) **35**, 27 (1974).

[22] F. Moussa and J. Villain, J. Phys. C **9**, 4433 (1976).

[23] D.R. Nelson and D.S. Fisher, Phys. Rev. B **16**, 4945 (1977).

[24] S.L. Menezes, A.S.T. Pires, and M.E. Gouvêa, Phys. Rev. B **47**, 12 280 (1993).

[25] F.G. Mertens, A.R. Bishop, G.M. Wysin, and C. Kawabata, Phys. Rev. Lett. **59**, 117 (1987); Phys. Rev. B **39**, 591 (1989).

[26] F.G. Mertens, A.R. Bishop, M.E. Gouvêa, and G.M. Wysin, J. Phys. C **8**, 1385 (1988); M.E. Gouvêa, G.M. Wysin, A.R. Bishop, and F.G. Mertens, Phys. Rev. B **39**, 11 840 (1989).

[27] G.M. Wysin, M.E. Gouvêa, and A.S.T. Pires, Phys. Rev. B **62**, 11 585 (2000).

[28] M. Krech and D.P. Landau, Phys. Rev. B **60**, 3375 (1999).